

9-23-2020

Evolution and mechanism of permeability of unconsolidated sandstone under high hydrostatic pressure compaction

Fu-jian YANG

University of Chinese Academy of Sciences, Beijing 100049, China

Da-wei HU

University of Chinese Academy of Sciences, Beijing 100049, China

Zhen-bao TIAN

Huadong Engineering Corporation Limited, China Power Engineering Consulting Group Corporation, Hangzhou ,Zhejiang 310014, China

Hui ZHOU

University of Chinese Academy of Sciences, Beijing 100049, China

See next page for additional authors

Follow this and additional works at: <https://rocksoilmech.researchcommons.org/journal>



Part of the [Geotechnical Engineering Commons](#)

Custom Citation

YANG Fu-jian, HU Da-wei, TIAN Zhen-bao, ZHOU Hui, LU Jing-jing, LUO Yu-jie, GUI Shu-qiang, . Evolution and mechanism of permeability of unconsolidated sandstone under high hydrostatic pressure compaction[J]. Rock and Soil Mechanics, 2020, 41(1): 67-77.

This Article is brought to you for free and open access by Rock and Soil Mechanics. It has been accepted for inclusion in Rock and Soil Mechanics by an authorized editor of Rock and Soil Mechanics.

Evolution and mechanism of permeability of unconsolidated sandstone under high hydrostatic pressure compaction

Authors

Fu-jian YANG, Da-wei HU, Zhen-bao TIAN, Hui ZHOU, Jing-jing LU, Yu-jie LUO, and Shu-qiang GUI

Evolution and mechanism of permeability of unconsolidated sandstone under high hydrostatic pressure compaction

YANG Fu-jian^{1,2}, HU Da-wei^{1,2}, TIAN Zhen-bao³, ZHOU Hui^{1,2}, LU Jing-jing^{1,2}, LUO Yu-jie^{1,2}, GUI Shu-qiang⁴

1. State Key Laboratory of Geomechanics and Geotechnical Engineering, Institute of Rock and Soil Mechanics, Chinese Academy of Sciences, Wuhan, Hubei 430071, China

2. University of Chinese Academy of Sciences, Beijing 100049, China

3. Huadong Engineering Corporation Limited, China Power Engineering Consulting Group Corporation, Hangzhou ,Zhejiang 310014, China

4. Changjiang Institute of Survey, Planning, Design and Research, Wuhan, Hubei430010, China

Abstract: The unconsolidated sandstone in hydrothermal geothermal field in Jiangnan basin is taken as the research object. The hydrostatic pressure is applied to a geostress equal to 12.5 MPa. After the deformation of sample is stabilised, the evolution and mechanism of the permeability of unconsolidated sandstone under the compaction of high hydrostatic pressure are studied, which can provide some suggestions for the selection of equipment operating parameters for the tailwater recharge process in the hydrothermal geothermal field. The results indicate that under high hydrostatic pressure compaction, the permeability of unconsolidated sandstone samples tends to be a constant valued of $4.0 \times 10^{-3} \mu\text{m}^2$ within the current range of 0.5 mL/min to 3.0 mL/min. The pressure difference between the two ends of the sample increases nonlinearly with time and the degree of nonlinearity gradually increases with the increase of flow rate, but eventually tends to be stabilised. In addition, the sample of unconsolidated sandstone forms a tubular erosion channel in the direction of penetration, extending to about 2/3 of the sample. Based on the stop time of particle transportation and the extension length of tubular erosion channel in the penetration direction, the average migration velocities of particles under different flow rates are determined. It is found that the particle migration velocity increases exponentially with the increase of flow rate, and the amount of microparticle migrated per unit time increases. When the pressure difference exceeds about 1/2 of the hydrostatic pressure, the sample presents erosion damage and upstream diameter shrinkage.

Keywords: high hydrostatic pressure; unconsolidated sandstone; permeability; suffusion; particle migration

1 Introduction

The water source heat pump (WSHP) is an efficient, recyclable, and clean energy technology, the principle of which is to extract heat from middle and deep aquifers with a relatively stable temperature (hydrothermal geothermal fields) for heating in winter or to absorb heat for cooling in the summer^[1]. The heat source currently used by the WSHP system is mainly concentrated in shallow low-and medium-temperature water sources on the earth's surface, with depths of less than 1,000 m, and most of the strata contain thick, unconsolidated sandstone containing fine particles formed during the Quaternary or Neogene. Having experienced only the mechanical compaction and cementation in the early diagenesis stage, the strata feature poor cementation degrees^[2-3]. To protect the ecology, the WSHP technology uses the principle of "heat extraction without water extraction." Therefore, the tail water should be recharged to the geothermal field in the same stratum through the recharge well. Consequently, the recharge

efficiency is of great significance for the heat supply capacity and economic benefit of the WSHP system.

Problems such as rapid rises in the recharge pressure and low recharge efficiencies due to blockages during the on-site recharge of a WSHP have become increasingly severe^[4]. In some thermal reservoirs, under a normal recharge state, the stable recharge rate is only 1/3 to 1/5 of the normal water withdrawal^[5], and the recharge efficiency of some recharge wells almost approaches 0% due to blockages, leading to the complete failure of the recharge well^[6]. The recharge blockages can be physical, chemical, or biological, among which, physical blockage occurs most frequently during the recharge process of the groundwater source heat pump. The primary reason is that the migrating suspended solids in the recharged water or the solid particles generated in the thermal reservoir under the hydrodynamic and hydrochemical actions block the pores of the sand layer, resulting in a decrease in the permeability of the thermal reservoir and an increase in the recharge pressure. In addition, Wang et al.^[6,7-9] studied the

Received: 17 December 2018

Revised: 30 April 2019

Supported by: National Natural Science Foundation of China (51479193, 51779252), Major Program of Technological Innovation of Hubei Province (2017AAA128) and CAS Pioneer Hundred Talents Program (2015).

First author: YANG Fu-jian, male, born in 1995, doctoral candidate, majoring in rock mechanics and engineering. E-mail: fjYangUCAS@163.com

Corresponding author: HU Da-wei, male, born in 1981, PhD, Professor, research interest: multi-field coupling of underground engineering. E-mail: dwhu@whrsm.ac.cn

impacts of the biological and chemical action on recharge blockages, believing that microorganisms and heavy metal ions such as calcium, iron, and manganese ions are the main factors resulting in the biological/chemical blockages and media permeability decline of a WSHP.

Moreover, the permeability characteristics of unconsolidated sandstone or gravel in oil reservoirs have been extensively studied. Using a self-developed seepage-erosion-stress coupling piping test apparatus, Luo et al. [10] studied the critical hydraulic gradient of unconsolidated gravel under different stress states, finding that the critical hydraulic gradient under isotropic stress was much higher than that under no confining pressure and slightly higher than that under triaxial compression. Hydrostatic and pore water pressures comprehensively affect the permeability characteristics of unconsolidated sandstone strata, and under constant hydrostatic pressure, the permeability will decrease irreversibly with the increase in pore pressure^[11-13]. During the extraction of heavy oil in strata with steam-driven unconsolidated sandstone, the migration of steam and concentrated liquids as well as hydrothermal reactions lead to an irreversible reduction in the permeability of unconsolidated sandstone strata^[14-17]. Schutjens^[18], Houseknecht^[19], and Alhomadhi^[20] et al. studied the influences of the compaction, cementation type, and particle size on the permeability characteristics of unconsolidated sandstone. Alhomadhi^[20] also worked out a new relationship between the permeability, porosity, and the above factors. Huo^[21] and Zhang^[22] et al. analyzed the effect of temperature on the permeability characteristics of unconsolidated sandstone strata, the experimental results of which showed that given the same water content, the permeability of unconsolidated sandstone increased with temperature. Furthermore, the stress path and the type and contents of clay minerals also affect the permeability characteristics of unconsolidated sandstone strata^[23-25].

Based on the studies described above, problems such as the rapid rise in the recharge pressure and low recharge efficiency due to blockages during the recharge have become increasingly severe in hydrothermal fields, and the permeability characteristics of unconsolidated sandstone are impacted by multiple factors. Nonetheless, in the previous studies, the confining pressures applied by the unconsolidated sandstone specimens were too small, and the stress states were different from the pressure of the overlying strata of the actual sandstone layer. Furthermore, with relatively few studies on the evolution of the permeability characteristics of unconsolidated sandstone over time, the evolution mechanism remains unclear. Therefore, with the recharge of tail water in unconsolidated sandstone strata in hydrothermal geothermal fields as the research subject, standard specimens were formed based on the water content and density of the sandstone layer. Specimens with a porosity close to that of the sandstone layer were chosen as the research objects, and hydrostatic pressure equal to the measured stress of

the overlying strata was applied. Once the deformation of the specimens stabilized, the evolution and mechanism of the permeability of unconsolidated sandstone under high confining pressure were studied under different recharge flows, providing suggestions for the selection of equipment parameters during the recharge process in hydrothermal fields.

2 Experiment overview

2.1 Specimen preparation

The specimens were extracted from the hydrothermal geothermal field in Jiangnan Oilfield, which was currently the largest WSHP project in central China. The unconsolidated sandstone was taken from the Neogene Guanghuasi Formation, which was overlaid with Quaternary sedimentary layers, with burial depths of 600–700 m and a poor cementation. With a porosity ranging from 24.9% to 43.8%, an average porosity of 36.5%, and a pressure coefficient (referring to the ratio of the original pore pressure of the stratum to the hydrostatic pressure of the stratum at the same depth) of about 1.0, the thermal reservoir was a normal pressure system.

The unconsolidated sandstone was mainly composed of quartz (59.25%), feldspar (14.48%), and clay minerals (26.27%). Featuring argillaceous cementation and a low cementation degree, most the extracted sandstone was unconsolidated (see Fig.1). Fig.2 shows the distribution of the particle sizes. According to the on-site geological data and the basic physical characteristics of sandstone, the unconsolidated sandstone extracted on site was used to form standard cylinder specimens with the same densities and water contents as those of the sandstone layer from which the material was extracted (see Fig.3(a)). The dimensions of the specimens were $\phi 50$ mm \times 100 mm (diameter \times height). The remoulded specimens were placed in a vacuum pump to be saturated for 24 h. During the saturation process, to prevent the specimens from becoming unconsolidated once exposed to water, the specimens were wrapped using a thermal shrinkable tube (Fig.3(b)). Table 1 shows the physical properties of the sandstone strata and sandstone.



Fig.1 Unconsolidated sandstone

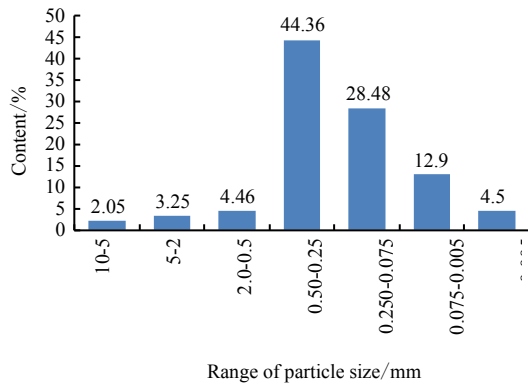
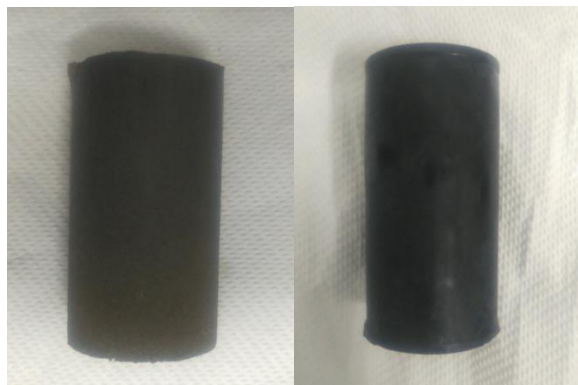


Fig.2 Particle size distribution of unconsolidated sandstone



(a) Specimen without thermal shrinkable tube (b) Specimens wrapped with thermal shrinkable tubes

Fig.3 Standard samples

Table 1 Physical properties of sandstone strata and sandstone

In-situ stress /MPa	Grain density /(g • cm ⁻³)	Saturated water content /%	Saturated density /(g • cm ⁻³)	Porosity /%
12.5	2.7	16.5	2.2	36.5

2.2 Testing apparatus

The core holder developed by the Institute of Rock and Soil Mechanics, Chinese Academy of Sciences, was used as the testing apparatus in this study. It consisted of three parts, i.e., a hydrostatic pressure chamber, a hydrostatic pressure loading and acquisition system, and a pore pressure loading and acquisition system. The pore pressure loading system was able to apply a pore pressure with a constant pressure and current. With a maximum of 45 MPa for pore pressure, and the hydrostatic pressure could be loaded to 60 MPa. Fig.4 shows the schematic diagram of the test apparatus.

2.3 Testing procedures and principles

To test the evolution and mechanism of the permeability of unconsolidated sandstone with time under high confining pressure, the test procedures were designed as follows:

- (1) The standard specimens with the same saturated water content and density as those of the sandstone layer were prepared. The specimen with a porosity close to that of the sandstone layer was selected and placed in a vacuum pump to be saturated for 24 h. Table 2 shows the physical parameters of the specimens.

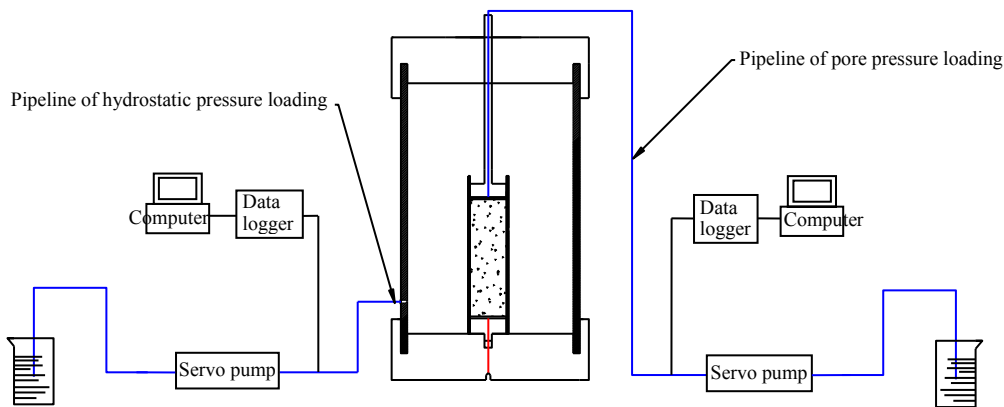


Fig.4 Schematic diagram of the experiment equipment

Table 2 Physical parameters of specimens

Specimen	Diameter /mm	Height /mm	Density /(g • cm ⁻³)	Saturated water content /%	Porosity /%
A	50.06	100.03	2.18	17.02	32.56
B	50.12	100.85	2.16	16.54	37.41
C	50.20	100.25	2.21	16.87	35.26
D	50.08	100.06	2.20	17.05	33.21
E	50.14	100.12	2.23	16.97	38.97

- (2) A saturated specimen was placed in the core holder. During the seepage process, radially oriented seepage plates

were placed at the upper and lower ends of the specimen (Fig.5). As the percolating fluid upstream of the pore pressure

reached the center of the seepage plate, the percolating fluid flowed to the surroundings along the radial guide groove, the flow rate gradually decreased, and the fluid flowed axially along the seepage holes in the groove. Once the hydrostatic pressure was applied to a constant value of 12.5 MPa and the deformation of the specimens stabilized, seepage tests were performed at a constant flow rate (0.5, 1.0, 2.0, 2.5, or 3.0 mL/min), and the changes in the pressure difference between the upstream and downstream were recorded in real time. Once the test ended, each pore pressure difference was substituted into the permeability equation to obtain the evolution behavior of the permeability. To ensure the flow regime in stability, the pore pressure difference was recorded once the water droplets uniformly flowed out from the water outlet of the core holder, and the pore pressure difference was recorded at regular intervals. The flow rate was selected such that the seepage flow rate during the actual recharge process on site was the same order of magnitude as the seepage flow rate during the test. The corresponding test design is shown in Table 3. The permeability was calculated using Darcy's law^[10]. The diagram of the measurement principle is shown in Fig.6, and the permeability was calculated using the following formula:

$$K = \frac{Q\mu L}{\Delta P A} \quad (1)$$

where K is the permeability of the specimen (μm^2), Q is the seepage flow rate (mL/min), μ denotes the dynamic viscosity coefficient of the fluid (1.005×10^{-3} Pa·s), ΔP represents the pore pressure difference between the specimens upstream and downstream (MPa), and A is the cross-sectional area of the specimen (cm^2).

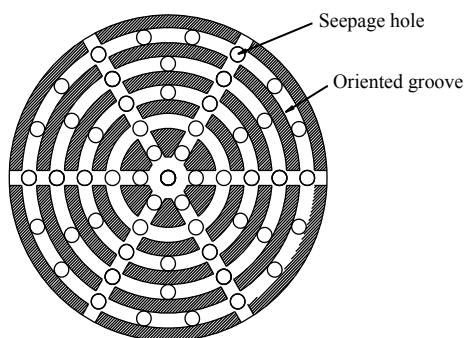


Fig.5 Permeation plate

Table 3 Test plans

Specimen	Seepage discharge /(mL · min ⁻¹)	Hydrostatic pressure /MPa
A	0.5	12.5
B	1.0	12.5
C	2.0	12.5
D	2.5	12.5
E	3.0	12.5

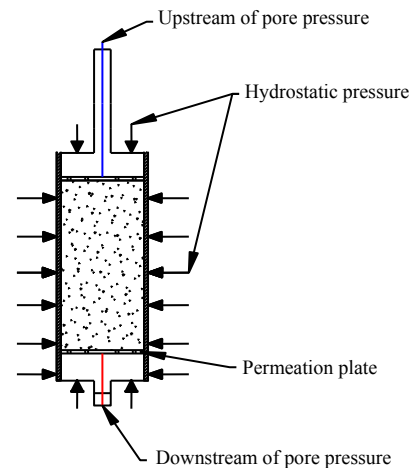


Fig.6 Mechanism diagram of permeability

3 Results and analysis

3.1 Evolution of permeability

The permeability of an unconsolidated sandstone stratum under a high geostress directly affects the heating capacity and recharge of a hydrothermal geothermal field, it is critical to fully understand the evolution and mechanism of the permeability characteristics of unconsolidated sandstone during the whole process of seepage under high hydrostatic pressure. Based on the actual site conditions, the high hydrostatic pressure (12.5 MPa) was applied, and the seepage test was conducted at different flow rates (0.5, 1.0, 1.5, 2.0, and 2.5 mL/min) to obtain the evolution characteristics of the permeability of unconsolidated sandstone over time, the results of which are shown in Fig.7.

Under different seepage flow rates, the permeability of the unconsolidated sandstone decreased non-linearly with time but eventually stabilized, and the stable permeability at different seepage flow rates approached a constant, i.e., $4.0 \times 10^{-3} \mu\text{m}^2$ (Figs.7 and 8). The time for the permeability of the unconsolidated sandstone to reach a stable value gradually decreased approximately linearly with the increase in the seepage flow rate (Fig.9). This indicated that the seepage flow rate affected the time for the sandstone layer to reach a stable permeability, but it had no effect on the final stable permeability. During seepage, the pressure difference between the two ends of the specimen increased non-linearly, and the degree of non-linearity increased gradually with the increase in the seepage flow rate. The pressure difference eventually approached a stable value with time (except for specimen E, which failed at a pressure difference of 6.55 MPa without achieving a stable pressure difference) and increased approximately linearly with the increase in the seepage flow rate, which agrees with Darcy's law (Fig.8).

As shown in Fig.8, under high hydrostatic pressures, the specimens exhibited the pore pressure gradient as high as 104–655 kPa/cm when the permeability was stable, which were

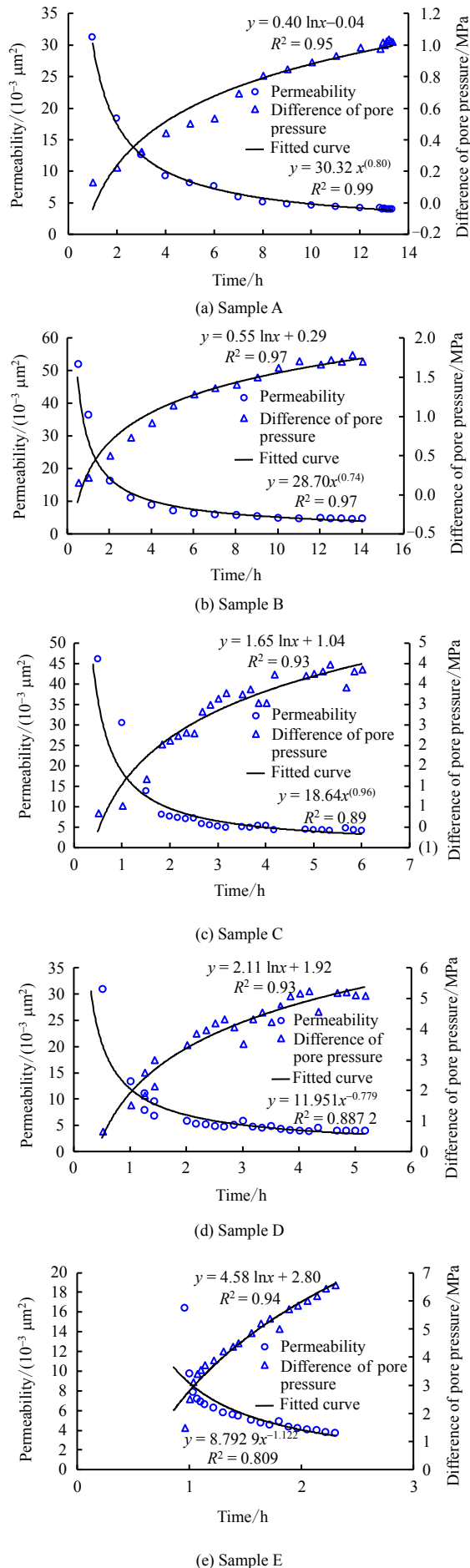


Fig.7 Evolution of sample permeability

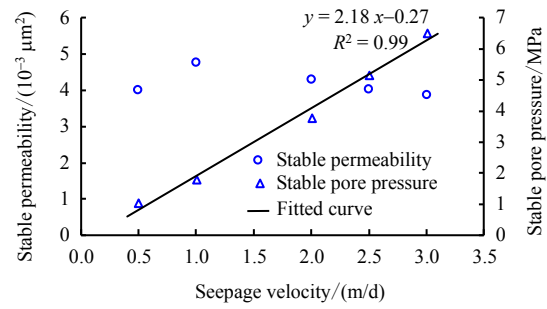


Fig.8 Evolution of stable permeability and stable pressure difference of unconsolidated sandstone

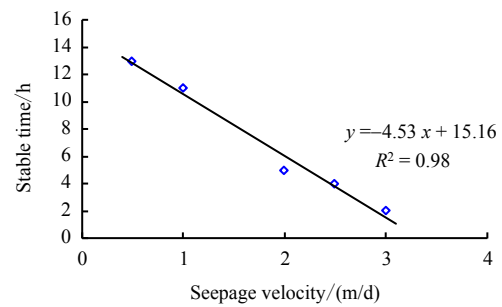


Fig.9 Time evolution of permeability stability of unconsolidated sandstone

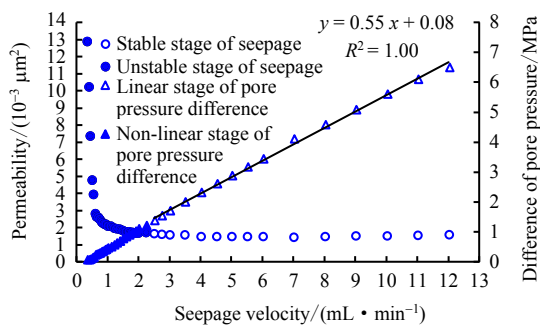
much higher than that of ordinary clay^[26-27]. Furthermore, under such a high pore pressure, only specimen E is in failure at a pore pressure gradient of 649 kPa/cm, and the other specimens remained intact. This phenomenon may have been caused by two factors. First, in previous studies on the critical pore pressure of cohesive or gravel soil, there was no confining pressure applied on the specimens, or the confining pressure was quite small. However, the results obtained by Luo et al.^[27-28] showed that the critical pore pressure of the specimens significantly increased after a confining pressure was applied. In this study, because the hydrostatic pressure of 12.5 MPa was applied to the specimens, the critical pore pressure increased significantly, and the specimens remained intact at a high pore pressure under the compaction of the hydrostatic pressure. Moreover, Xiong et al.^[12] studied the evolution of the permeability characteristics of unconsolidated sandstone reservoirs under compaction. With a hydrostatic pressure of 30 MPa was applied to the specimens, the pore pressure difference between the two ends of the specimens reached 5–15 MPa during the seepage process, the pore pressure gradient was as high as 796–2,388 kPa/cm, but the specimens remained intact. Second, the evolution of the permeability characteristics of the unconsolidated sandstone during the recharge process of the hydrothermal geothermal field was simulated in this study. Blockage is an inevitable phenomenon in the current tail water recharge process^[29-30], and the rapid rise of the recharge pressure and low recharge efficiency are also common problems in actual engineering^[4]. Nevertheless, in actual engineering, when the pressure rises to a certain level, measures such as well washing and acidification will be taken to reduce the recharge pressure. For example, in a study conducted by

Dai et al.^[4], during the tail water recharge of the sandstone layer in the hydrothermal geothermal field of the Shengli Oilfield, the maximum recharge pressure reached 3.7 MPa, and the recharge pressure dropped to 0.6 MPa after acidification. However, the recharge of the tail water was simulated in this study to determine the permeability characteristics and mechanism of unconsolidated sandstone during the recharge process. Because the test was not stopped after the recharge pressure reached a certain level, the critical pore pressure gradient reached values as high as 104–655 kPa/cm.

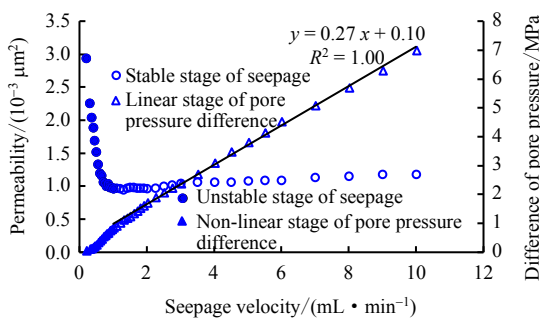
Furthermore, under the combined effect of such a high pore pressure and hydrostatic pressure, whether the permeability can be calculated using the linear Darcy's law and whether the flow regime is in stability must be addressed. Therefore, based on the above studies, a hydrostatic pressure of 12.5 MPa was applied to specimens F and G (Table 4) with similar physical properties to explore the permeability characteristics of unconsolidated sandstone at different seepage flow rates. The results are shown in Fig.10.

Table 4 Physical parameters of specimens

Specimen	Diameter /mm	Height /mm	Density /($\text{g} \cdot \text{cm}^{-3}$)	Saturated water content /%	Porosity /%
F	50.16	100.21	2.19	17.00	36.25
G	50.09	100.17	2.21	16.80	35.85



(a) Sample F



(b) Sample G

Fig.10 Evolution of sample permeability at different flow rates for specimens F, G

As shown in Fig.10, under a hydrostatic pressure of 12.5 MPa, specimens F and G failed once their pore pressure gradients reached 648 and 699 kPa/m, respectively. Except for the unstable state of seepage at the beginning of the test, the

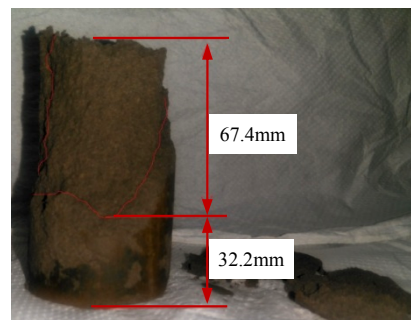
flow rate and the pressure difference at the two ends of the specimens were approximately linearly related, and the permeability then approached a stable value of about $1.0 \times 10^{-3} \mu\text{m}^2$, indicating that the unconsolidated sandstone specimens in this study still complied with the linear Darcy's law and met the steady-state conditions of Darcy's law under the combined effects of a high pore pressure and hydrostatic pressure. In addition, when studying the oil-water two-phase low-speed non-Darcy flow in a low permeability oilfield, Shi^[31] found that the non-Darcy flow produced by single-phase water flow occurred at a limited permeability of $1.0 \times 10^{-3} \mu\text{m}^2$. Displaced by a single-phase water flow of 0.25 mL/min, the pore pressure gradient reached 1,000 kPa/cm, which further verified that the unconsolidated sandstone specimens studied in this study still complied with the linear Darcy's law under the combined effect of a high pore pressure and hydrostatic pressure.

3.2 Mechanism of permeability evolution

After the test, a tubular erosion channel was observed in the unconsolidated sandstone specimens along the direction of seepage, as shown in Fig.11(a). After the thin layer outside the erosion channel was peeled off, it was observed that the erosion channel penetrated to 2/3 of the specimens, as shown in Fig.11(b). This indicated that under the seepage effect, unconsolidated sandstone in the fine particles moved through the pores and throats to form tubular subsurface erosion channels^[32]. Most fluids and fine particles preferentially percolated and migrated via the erosion channels, which were then expanded and extended.



(a) Circumferential erosion channel



(b) Axial erosion channel

Fig.11 Erosion channel

To further understand the migration of these particles, the specimens that formed erosion channels were axially divided

into three sections, namely the upper, middle, and lower sections, for particle size analysis. According to the analysis results of the particle size (Fig.12), the contents of particles with diameters less than 0.075 mm gradually increased from the upper parts to the lower parts of the specimens, while there was no evident migration pattern of the remaining particles. The contents of particles with diameters less than 0.075 mm in the upper parts of the specimens were lower than that in the sandstone layer. The contents of particles with diameters less than 0.075 mm in the middle parts of the specimens were close to that in the sandstone layer. The contents of particles with diameters less than 0.075 mm in the lower parts of the specimens were higher than that in the sandstone layer. Under different seepage velocities, the contents of particles with diameters less than 0.075 mm in the same parts of the specimens were quite close, which agreed with the conclusion drawn by Zhang et al. [33] by analyzing the particle sizes of soil layers at different heights after studying the seepage erosion caused by pipeline damage. This implies that within the range of currently studied seepage flow rates, particles with diameters smaller than 0.075 mm migrated from the upper parts to the lower parts of a specimen via the erosion channels, pores, and throats, and eventually accumulates at the bottom regions of the specimen. Moreover, the total migration of movable particles was not affected by the seepage flow rate.

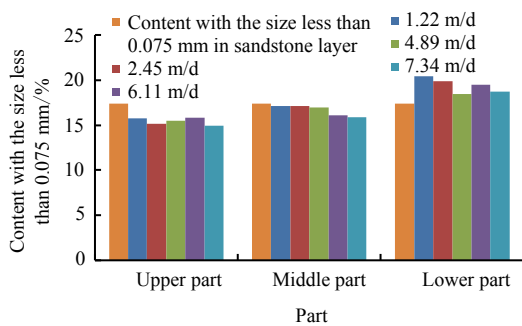


Fig.12 Analysis of particle size in different parts of sample

As indicated by the above analysis, during the seepage process, the pressure differences between the two ends of the specimens gradually increased, and once the pressure difference reached the critical pore pressure gradient of the fine particles^[34-37], particles with diameters less than 0.075 mm migrated through the pores, forming a tubular erosion channel that gradually expanded and extended as the seepage progressed. Under the hydrostatic pressure, the erosion channel would be further compacted as it extended and expanded. Gradually trapped in the erosion channel during the migration process, the particles would gradually block the tubular erosion channel. As the seepage resistance increased, the permeability would progressively decrease, and the pressure difference between the two ends of the specimens would keep increasing until the particles migrated to the bottom of the specimens. The fine particles were limited by the bottom boundary conditions and were unable to flow out from the bottom regions of the specimens. The pores were thus blocked, leading to a decrease

in the permeability and an increase in the pressure differences between the two ends of the specimens. As most of the movable fine particles were deposited at the bottom regions of the specimens, once the migration stopped, the permeabilities and pressure differences at the two ends of the specimens gradually became stable. Moghadasi et al.^[38] observed the same phenomenon while studying the migration patterns of particles in a water-driven unconsolidated sandstone layer. As mentioned in Section 3.1, the permeability gradually decreased with time, while the pressure difference gradually increased, and eventually stabilized. The particles inside the specimens gradually migrated during the seepage process, blocking the subsurface erosion channels, and eventually accumulating at the bottom of the specimens, which is also one of the reasons the pore pressure gradient at both ends of the specimens were as high as 104–655 kPa/cm.

According to the above analyses, during the seepage of the unconsolidated sandstone, particles migrated along the direction of seepage. Therefore, a correct understanding of the migration velocities of particles at different seepage velocities would help to further comprehend the evolution mechanism of the permeability characteristics. When most of the movable fine particles stop moving, the permeability would gradually become stable. Hence, the time when the particles stopped moving was defined as the time when the permeability became stable. In this study, if there was a difference less than 5% between the current permeability and the average of all subsequent permeabilities, the permeabilities of the specimens was considered to be stable. The distance of the particle migration could be determined based on the expanded and extended lengths of the tubular erosion channel along the seepage direction. Therefore, based on the time when the particles stopped moving and the particle migration distance, the average migration velocity of the movable fine particles at different seepage velocities was defined as follows (Fig.12):

$$v_k = \frac{L_{H}}{T_w} \tag{2}$$

where v_k is the average migration velocity of the particles (m/d); L_{H} denotes the length of the tubular erosion channel extending along the seepage direction (m); and T_w refers to the time at which the particles stopped moving, i.e., the time when the permeability was stabilized (d).

Fig.13 shows the evolution of the seepage flow rate, which is calculated using the equation recommended by the oil and gas industry standard^[39]:

$$v = \frac{14.4Q}{A\phi} \tag{3}$$

where v is the seepage flow rate (m/d), and ϕ is the porosity (%) of the specimen.

As shown in Fig.13, as the seepage velocity increased, the migration speed of the unconsolidated sandstone particles surged exponentially. In addition, based on the analysis of the particle sizes in different regions of the specimens, the amount of total migration of movable particles was not influenced by the seepage flow rate. In other words, as the seepage flow rate

increased, the migration amount within a unit time as well as the migration velocity of the fine particles increased, resulting in more severe blockages of the seepage channels and increasing the seepage resistance. This effectively explained why the time for the permeability to reach a stable value gradually decreased with the increase in the seepage flow rate (Fig.9), but the stable permeability remained basically constant (Fig.8), and the stable pressure difference at both ends of the specimens gradually increased with the increase in the seepage flow rate (Fig.8).

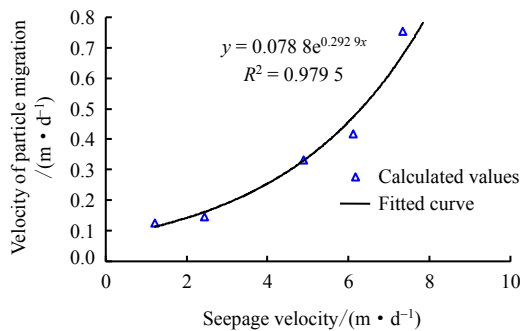


Fig.13 Particle migration velocity at different flow rates

3.3 Failure of specimens

At a seepage flow rate of 3.0 mL/min, Specimen E was failure as the pressure differences between the upstream and downstream regions of the specimens reached 6.55 MPa, whereas no failure was found in other samples with smaller seepage flow rates. Hence, another permeability test with a seepage flow rate of 3.0 mL/min was performed on Specimens E-1 and E-2, the results of which show that Specimens E-1 and E-2 failed when the pressure difference between the upstream and downstream reached 6.58 and 6.67 MPa, respectively. Diameter shrinkage failure also occurred in the upstream regions of the specimens. Fig.14 shows the failure mode. In addition, when the permeability characteristics of Specimens F and G were studied under different seepage flow rates, it was found that diameter shrinkage failure occurred when the pressure difference between the upstream and downstream regions of Specimens F and G reached 6.48 and 6.99 MPa, respectively. Thus, the critical pressure differences at the time of failure of the different specimens under the compaction of a high hydrostatic pressure of 12.5 MPa were determined (Fig.15).

As shown in Fig.15, under the same hydrostatic pressure of 12.5 MPa, the critical pore pressure difference of the unconsolidated sandstone specimens composed of natural-sized particles ranged from 6.48 to 6.99 MPa, which implies that when the pore pressure difference between the upstream and downstream regions of the specimens exceeded about 1/2 of the hydrostatic pressure, the specimens would be in failure, with diameter shrinkage occurring upstream. There were mainly three reasons that diameter shrinkage occurred in the upper parts of the specimens. First, under the seepage pressure differences, the specimens have seepage compression^[32].

Consequently, the fine particles that filled between the skeleton structures migrated and accumulated at the bottoms of the specimens, which created voids between the upper skeleton structures, thereby weakening the deformation resisting capability of the skeleton structures^[40]. Meanwhile, the fine particles between the bottom skeleton structures became more dense, and the bottom skeleton structures became more resistant to deformation. Second, as the internal pore pressures of the specimens increased sharply, the particles within the upper structures of the specimens, under the action of larger pore pressures, were deformed and dislocated. The third cause was the compression effect of the applied hydrostatic pressure. As a result, under the combined effects of voids in the skeleton structure, the deformation and dislocation of the skeleton particles^[41], and the hydrostatic pressure, the compression deformation and diameter shrinkage occurred in the upper parts of the specimens.

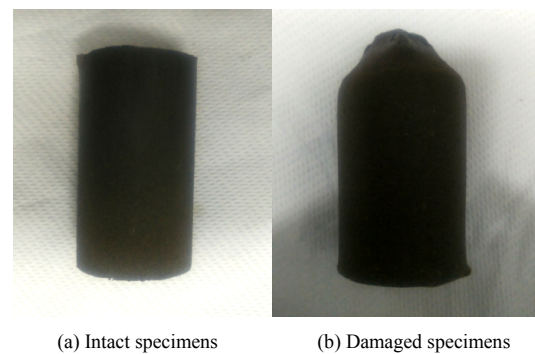


Fig.14 Failure mode of sample

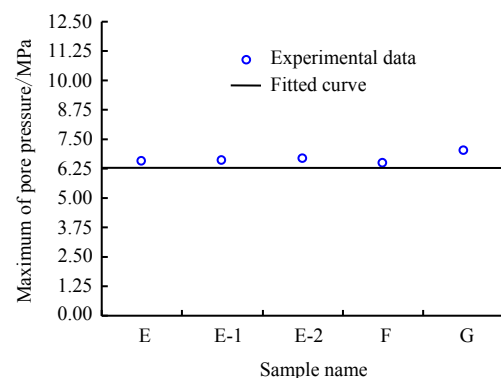


Fig.15 Maximum pressure difference at sample failure

4 Conclusions

In this study, the unconsolidated sandstone taken from the hydrothermal geothermal field in Jiangnan Basin were used to prepare standard specimens based on the saturated water content, density, and porosity of the unconsolidated sandstone layer in field. A high hydrostatic pressure of 12.5 MPa, which is equal to the actual pressure of the overlaying strata was applied. The permeability characteristics and evolution mechanism of the unconsolidated sandstone under high hydrostatic pressure compaction were explored, and the following conclusions were

obtained:

(1) Under the compaction of high hydrostatic pressure, the permeability of the unconsolidated sandstone and the pressure difference between both ends of the specimens varied nonlinearly with time and finally stabilized, with the stable permeability approaching a constant of $4.0 \times 10^{-3} \mu\text{m}^2$. The stable pressure difference increased approximately linearly with the increase in the seepage flow rate, which agreed with Darcy's law.

(2) The average migration velocity of the particles at different seepage flow rates was defined based on the time when the particles stopped moving and the length of the tubular erosion channel. The migration velocity of the particles surged exponentially with the increase in the seepage flow rate. By analyzing the sizes of particles in different parts of the specimens, it was found that the total migration of movable particles was not affected by the seepage flow rate, but the migration number of fine particles per unit time increased. It should be noted that the average migration velocity of the particles defined in this study refers to the average value of the migration velocities of all movable fine particles. It should be especially pointed out that the time when the particles stopped moving was estimated based on the correlation between the blockage and permeability of the particles rather than an actually measured physical quantity, which means that there were certain errors and there was no evidence to support the microscopic real-time monitoring. However, it is undeniable that the method of defining the migration velocity of particles in this study is scientifically grounded, and this method contributes to the further understanding of the evolution mechanism of the permeability characteristics of unconsolidated sandstone.

(3) Under the compaction of high hydrostatic pressure of 12.5 MPa, the maximum pore pressure difference of the unconsolidated sandstone specimens composed of natural-sized particles ranged from 6.48 to 6.99 MPa, which implied that when the pore pressure difference between the upstream and downstream of the specimens exceeded about 1/2 of the hydrostatic pressure, the specimens would be in failure, with diameter shrinkage occurring upstream.

Because the specimens taken from the site were unconsolidated, the unconsolidated sandstone specimens used in this study were remoulded. The specimens were prepared based on the density, water content, and porosity of the actual thermal reservoir, yet the specimens were still different from the actual thermal reservoir in terms of features such as the pore structure and cementation degree. Furthermore, due to the differences between the experimental and actual project conditions, the flow regime in the test slightly differed from the actual flow state, which is an inevitable problem of simulating the project site for laboratory tests. Hence, due to the differences between the laboratory conditions and the actual engineering conditions, the conclusions drawn in this study

cannot be directly applied to the project site. Nonetheless, some suggestions can be provided for selecting relevant parameters during the recharge process of the hydrothermal geothermal fields according to the phenomena found in the experiment. For instance, within the range of seepage flow rates explored in this study, the stable permeability of unconsolidated sandstone specimens under the compaction of a high hydrostatic pressure was not affected by the seepage flow rate, but the pore pressures of the specimens would increase. When the pore pressure increases to a certain value, the specimens will fail. Therefore, it is recommended that large flow recharge is not blindly pursued during the actual tail water recharge process of the hydrothermal geothermal field in Jiangnan Oilfield. Otherwise, the pore pressure of the geothermal reservoir will increase sharply, subsurface erosion will occur, and fine particles will accumulate at the far end, resulting in a low recharge efficiency, which may cause deformation and subsidence of the ground in some cases. Once the tail water recharge pressure is too high during the recharge process, applicable measures must be taken immediately to reduce the recharge pressure to ensure that the recharge well can be effectively used for a long time.

References

- [1] OMER A M. Ground-source heat pumps systems and applications[J]. *Renewable and Sustainable Energy Reviews*, 2008(12): 344-371.
- [2] XIE Yi-ting. Research on change of in-situ permeability near wellbore in unconsolidated sandstone reservoir with sand management[D]. Chengdu: Southwest Petroleum University, 2017.
- [3] LIU Hong-zhan, TIAN Yuan, YANG Po. A discussion of the construction technology of pumping and injection wells in the fine particle sediment distribution area[J]. *Hydrogeology & Engineering Geology*, 2017, 44(1): 36-40+56.
- [4] DAI Qun, WANG Cong, LUO Yang, et al. Research on sandstone geothermal reservoir reinjection plugging mechanism and measures against it[J]. *Advances in Fine Petrochemicals*, 2017, 18(6): 10-13.
- [5] LIN Jian-wang, ZHAO Su-min. An analysis of the reinjection attenuation of the Guantao group geothermal reservoir in the Tianjin Area[J]. *Hydrogeology & Engineering Geology*, 2010, 37(5): 133-136.
- [6] WANG Di, WEI Wei. Research on microbial blockage mechanism in water source heat pump recharge[J]. *Construction and Budget*, 2010, 37(5): 133-136.
- [7] SUN Y, MIAO L W. Current situation investigation and prospect analysis of artificial recharge of ground water in Beijing city[J]. *Hydrogeology and Engineering Geology*, 2001(1): 21-23.
- [8] ALBRECHTSEN H J, WINDING A. Microbial biomass

- and activity in subsurface sediment from Vejen, Denmark[J]. *Microbial Ecology*, 1992, 23(3): 303-317.
- [9] KANG Han, LI Ling, PAN Jun, et al. Research and prospects of groundwater source heat pump recharge blockage caused by suspended particles[J]. *Construction and Budget*, 2018(5): 61-63.
- [10] LUO Yu-long, WU Qiang, ZHAN Mei-li, et al. Development of seepage-erosion-stress coupling piping test apparatus and its primary application[J]. *Chinese Journal of Rock Mechanics and Engineering*, 2013, 32(10): 2108-2114.
- [11] XIONG Y, XU H, WANG Y, et al. The variation mechanism of petrophysical properties and the effect of compaction on the relative permeability of an unconsolidated sandstone reservoir[J]. *Marine and Petroleum Geology*, 2018(92): 754-763.
- [12] XIONG Y, XU H, WANG Y, et al. Fluid flow with compaction and sand production in unconsolidated sandstone reservoir[J]. *Petroleum*, 2018, 4(3): 358-363.
- [13] ZHOU Wen-sheng, XIONG Yu, XU Hong-guang, et al. Physical property and seepage characteristics of unconsolidated sandstone under re-compaction[J]. *Petroleum Drilling Technology*, 2015, 43(4): 118-123.
- [14] BAGCI S, KOK M V, TURKSOY U. Determination of formation damage in limestone reservoirs and its effect on production[J]. *Petroleum Science and Engineering*, 2000, 28(1): 1-12.
- [15] DIABIRA I, CASTANIER L M, KOVSCEK A R. Porosity and permeability evolution accompanying hot fluid injection into diatomite[J]. *Petroleum Science and Technology*, 2001(19): 1167-1185.
- [16] SCHEMBRE J M, KOVSCEK A R. Thermally induced fines mobilization: its relationship to wettability and formation damage[C]//Proceeding Soft the SPE 86937, March16–18, 2004. Bakersfield: [s. n.], 2004: 1-16.
- [17] PANG Z X, LIU H Q. The study on permeability reduction during steam injection in unconsolidated porous media[J]. *Petroleum Science and Engineering*, 2013(106): 77-84.
- [18] SCHUTJENS P M T M, SAYERS C, WHITWORTH J H. Production-induced compaction of the Brent field: an experimental approach[J]. *SPE Formation Evaluation*, 1996, 11(2): 99-107.
- [19] HOUSEKNECHT D W. Assessing the relative importance of compaction processes and cementation to reduction of porosity in sandstones[J]. *The American Association of Petroleum Geologists Bulletin*, 1989, 71(6): 633-642.
- [20] ALHOMADHI E S. New correlations of permeability and porosity versus confining pressure, cementation, and grain size and new quantitatively correlation relates permeability to porosity[J]. *American Journal of Geosciences*, 2014(7): 2871-2879.
- [21] HUO D, BENSON S M. Experimental investigation of stress-dependency of relative permeability in rock fractures[J]. *Transport Porous Media*, 2016, 113(3): 567-590.
- [22] ZHANG L H, TONG J, XIONG Y, et al. Effect of temperature on the oil-water relative permeability for sandstone reservoirs[J]. *International Journal of Heat and Mass Transfer*, 2017: 535-548.
- [23] NGUYEN V H, GLAND N, DAUTRIAT J. Compaction permeability evolution and stress path effects in unconsolidated sand and weakly consolidated sandstone[J]. *International Journal of Rock Mechanics and Mining Sciences*, 2014(67): 226-239.
- [24] MONFARED A K, ROTHENBURG L. Poro-elastoplastic response of an unconsolidated formation confined with stiff seal rocks under radial injection[J]. *International Journal for Numerical and Analytical Methods in Geomechanics*, 2016, 40(13): 1799-1826.
- [25] KIM C, LEE J. Experimental study on the variation of relative permeability due to clay minerals in low salinity water-flooding[J]. *Petroleum Science and Engineering*, 2017(151): 292-304.
- [26] WU Meng-xi, GAO Gui-yun, YANG Jia-xiu, et al. Research on prediction method of critical gradient for piping of sand and gravel soils[J]. *Rock and Soil Mechanics*, 2019, 40(3): 861-870.
- [27] LUO Yu-long, WU Qiang, ZHAN Mei-li, et al. Study of critical piping hydraulic gradient of suspended cut-off wall and sand gravel foundation under different stress states[J]. *Rock and Soil Mechanics*, 2012, 33(Suppl.1): 73-78.
- [28] YANG Jia-zhi, LIU Xing-xing, SHENG Jin-chang. Experimental investigation of the influence of confining pressure on piping in sandy gravel foundation[J]. *Journal of North China University of Water Resources and Electric Power (Natural Science Edition)*, 2014, 35(5): 16-19.
- [29] ZHAO Jun, LIU Quan-sheng, ZHANG Cheng-yuan. Experimental study of particles clogging in ground source heat pump[J]. *Rock and Soil Mechanics*, 2013, 34(11): 3249-3253.
- [30] HE Man-chao, LIU Bin, YAO Lei-hua, et al. Study on theory of seepage field around geothermal production-reinfection doublets wells[J]. *Journal of China University of Mining & Technology*, 2004, 33(3): 245-248.
- [31] SHI Jing-ping. Study on oil-water two-phase low-speed non-Darcy flow in low permeability oilfield[D]. Chengdu: Chengdu University of Technology, 2006.
- [32] LI Xi-an, CHEN Wen-jun, DENG Ya-hong, et al. Formula

- derivation of the critical condition of sub-ground erosion[J]. *Research of Soil and Water Conservation*, 2010, 17(5): 217-221.
- [33] ZHANG Dong-mei, DU Wei-wei, GAO Cheng-peng. Model test of seepage erosion caused by pipeline damage in gap grading sand[J]. *Chinese Journal of Geotechnical Engineering*, 2018, 40(11): 2129-2135.
- [34] LIU Zhong-yu, LE Jin-chao, MIAO Tian-de. Capillary-tube model for piping in non-cohesive soils and its application[J]. *Chinese Journal of Rock Mechanics and Engineering*, 2004, 23(22): 3871-3876.
- [35] LIU Zhong-yu. Critical hydraulic gradient for piping in noncohesive soils[J]. *Journal of Zhengzhou University (Engineering Science)*, 2003, 24(4): 67-71.
- [36] MAO Chang-xi, DUAN Xiang-bao, WU Liang-ji. Study of critical gradient of piping for various grain sizes in sandy gravels[J]. *Rock and Soil Mechanics*, 2009, 30(12): 3705-3709.
- [37] TAO Gao-liang, LI Jin, ZHUANG Xin-shan, et al. Seepage failure experiment of sandy soil caused by leakage of underground water pipe[J]. *Journal of Water Resources and Architectural Engineering*, 2018, 16(1): 97-102.
- [38] MOGHADASI J, MÜLLER-STEINHAGEN H, JAMIALAHMADI M. Theoretical and experimental study of particle movement and deposition in porous media during water injection[J]. *Journal of Petroleum Science and Engineering*, 2004, 43(3): 163-181.
- [39] National Energy Administration of China. SY/T 5358–2010 Formation damage evaluation by flow test[S]. Beijing: Petroleum Industry Press, 2010.
- [40] MARI S, REIKO K. Laboratory testing for evaluation of the influence of a small degree of internal erosion on deformation and stiffness[J]. *Soils and Foundations*, 2018, 58(3): 547-562.
- [41] YU Zi-wang. Research on multiphase-multicomponent THCM coupling mechanism and its application[D]. Changchun: Jilin University, 2013.